LETTER

Exploiting RIS-Aided Cooperative Non-Orthogonal Multiple Access with Full-Duplex Relaying

Guoqing DONG[†,††], **Zhen YANG**[†a)], **Youhong FENG**[††], ***Nonmembers*, *and* Bin LYU**[†], ***Member***

SUMMARY In this paper, a novel reconfigurable intelligent surface (RIS)-aided full-duplex (FD) cooperative non-orthogonal multiple access (CNOMA) network is investigated over Nakagami-*m* fading channels, where two RISs are employed to help the communication of paired users. To evaluate the potential benefits of our proposed scheme, we first derive the closed-form expressions of the outage probability. Then, we derive users' diversity orders according to the asymptotic approximation at high signal-to-noise-ratio (SNR). Simulation results validate our analysis and reveal that users' diversity orders are affected by their channel fading parameters, the self-interference of FD, and the number of RIS elements.

key words: *reconfigurable intelligent surface, full-duplex, cooperative non-orthogonal multiple access, outage probability*

1. Introduction

Reconfigurable intelligent surface (RIS) has been considered as an evolving technology for the sixth generation (6G) communication as it can intelligently adjust the wireless propagation environment. Specifically, an RIS consists of numerous low-cost passive elements, which are capable of electronically adjusting the magnitude and phase shifts of the reflected signals [1], [2]. Based on this characteristics, RIS has been widely used in communication systems to improve energy efficiency, spectral efficiency, and service coverage. For instance, in [3], the passive beamforming at the RIS and the active beamforming at the base station (BS) were jointly optimized to minimize the total transmit power. In [4], a multi-user multiple-input single-output RIS-aided system was considered, and a joint active and passive beamforming scheme was proposed to maximize the weighted sum rate. On the other hand, NOMA has also been envisaged as a promising technology to improve networks' spectral efficiency since it can serve multiple users with one time/bandwidth resource block [5], [6]. Furthermore, by employing the prior information available in NOMA, cooperative NOMA (CNOMA) is explored to gain a higher diversity order and coverage extension, where the near NOMA user acts as a decode-and-forward (DF) relaying to help the communication of the far NOMA user. Specifically, a full-duplex (FD) device-to-device-aided CNOMA system was proposed in [7] to improve the outage performance of the far user in a NOMA user pair. In [8] and [9], the near user was employed as an FD relaying for the far user when there exist no direct links from the BS to the far user.

Inspired by the aforementioned advantages of RIS and NOMA (or CNOMA) techniques, some recent works have integrated them for performance enhancement. In [10], a simple design of the RIS-aided NOMA network was first investigated, where the outage probability (OP) of cell-edge users is derived with 1-bit coding. Considering the RIS is pre-deployed in practical, the RIS-involved channels can be either non-light of sight (NLoS) or light of sight (LoS). With this characteristic, the authors in [11] further investigated the performance of the RIS-aided NOMA network over Nakagami-*m* fading channels, and it revealed the superiority of employing the RIS in terms of the diversity order. In [12], an RIS-aided half-duplex (HD) CNOMA system was first investigated to minimize the total transmit power, where one RIS is adopted and the minimum value occurs when the RIS is close to the far NOMA user. Furthermore, compared with the RIS-aided HD CNOMA scheme, the RIS-aided FD CNOMA scheme consumed less transmit power even in the case of the high residual self-reference (SI) at near NOMA user [13].

The aforementioned works [12] and [13] only employed one RIS, which can serve both the near user and the far user. However, the far user is always at the edge of the cell and far away from the BS and the near user. It is very likely that one RIS can not be able to serve the two users simultaneously. In addition, since the far user is far away from the BS, it always receives very weak signals from the BS. Similarly, the RIS near it suffers from this problem. Thus, to achieve effective signal transmissions for both NOMA users, we propose a novel RIS-aided FD CNOMA network, where the near user acts as an FD relay, and it can simultaneously receive its own messages from the BS and forward the decoded signals to the far user. Moreover, two RISs are employed to help the communication of paired users, respectively, due to the physical obstacles between the BS and users. On the other hand, the works in [12] and [13] only investigated the energy efficiency of RIS-aided CNOMA systems, without evaluating system transmit reliability. Meanwhile, the works in [10] and [11] only evaluated the transmit reliability of RIS-aided NOMA networks, without considering the impact of cooperative relaying schemes. To bridge this gap, we investigate the transmit reliability of our proposed RIS-aided CNOMA

Manuscript received August 17, 2022.
Manuscript revised November 20, 2022.
Manuscript publicized January 6, 2023.

[†]The authors are with School of Communications and Information Engineering, Nanjing University of Posts and Telecommunications, Nanjing 210003, China.
[††]The authors are with School of Physics and Electronic Information, Anhui Normal University, Anhui 241000, China.
a) E-mail: yangz@njupt.edu.cn

DOI: 10.1587/transfun.2022EAL2067

Copyright © 2023 The Institute of Electronics, Information and Communication Engineers

system and have the following contributions.

• We propose a novel RIS-aided FD CNOMA network, where the near user acts as an FD for the far user when receiving its own messages, and two RISs are employed to establish corresponding reflecting links for the paired users respectively.

• We consider the more general Nakagami-m fading channels. Under this setup, we first analyze the corresponding channel statistics of reflecting links with optimal phase shifts. Then, we derive the closed-form expressions of the OP for both users. To gain more insights, we further derive the asymptotic OP at high signal-to-noise-ratio (SNR) and then obtain the diversity orders.

• Simulation results are provided to validate our analysis. It is demonstrated that users' OPs can be significantly reduced by increasing the number of RIS elements. In addition, the diversity orders are affected by the number of RIS elements, the SI of FD, and Nakagami fading parameters.

2. System Model

As shown in Fig. 1, we consider an RIS-aided FD CNOMA system consisting of a base station (BS), two RISs (R_1 and R_2), and two users (U_1 and U_2), where the near user U_1 is enabled to act as an FD relay for the far user U_2 when receiving its own messages. In particular, the DF protocol is employed at U_1 to decode and forward information to U_2. The two users form a classical two-user NOMA group, and it can be extended to multi-user scenarios by employing user paring principles [5]. Moreover, the BS and U_2 are each equipped with one single antenna, while U_1 is with two antennas. We assume that the direct links, i.e., BS-U_1 (U_2) and U_1-U_2, are unavailable due to severe physical obstacles†. RISs are employed to build signal transmissions between them. Specifically, since the optimal location for the RIS deployment is near the BS or the user [3], we assume that R_1 is located near the BS and helps U_1 receive signals from the BS, and R_2 is located in the vicinity of U_2 and helps U_2 communicate with the cooperative relaying user, i.e, U_1. The two RISs are far away from each other, so the reflecting interference between them can be ignored. In addition, we assume R_i has N_i individual passive elements, and their corresponding reflection-coefficient matrix can be denoted by $\mathbf{\Theta}_i = diag\{\beta_{i,1}e^{j\theta_{i,1}}, \beta_{i,2}e^{j\theta_{i,2}}, \ldots \beta_{i,N_i}e^{j\theta_{i,N_i}}\}$, where $i \in \{1,2\}$, $\beta_{i,n_i} \in (0,1]$ and $\theta_{i,n_i} \in [0,2\pi)$ denote the magnitude and phase-shift of the n_ith element of RIS i, respectively ($n_i = 1,2,\ldots N_i$) [14], [15]. Without loss of generality, we set $\beta_{i,n_i} = 1$ to achieve better signal transmission performance.

2.1 Channel Model

We assume that all channels experience quasi-static flat fading, and the channel state information (CSI) can be fully estimated at the BS [3]. In addition, since RISs are pre-deployed, the BS-RIS and RIS-user links may be LoS or NLoS. With this consideration, we assume that all channels follow the Nakagami-m model. Specifically, the BS-R_1 and U_1- R_2 channels are denoted by $\mathbf{G}_i \in \mathbb{C}^{N_i \times 1}$ ($i \in (1,2)$) with the fading parameter m_{G_i}. The R_1-U_1 and R_2-U_2 channels are denoted by $\mathbf{g}_i \in \mathbb{C}^{1 \times N_i}$ with the fading parameter m_{g_i}. Particularly, $m_\zeta = 1$ represents the links are NLoS, while $m_\zeta > 1$ indicates the links are LoS ($\zeta \in \{G_i, g_i\}$).

†If the direct links between BS-U_2 and U_1-U_2 exist, U_2 can combine signals from both the BS and U_1. Accordingly, the reliability performance of U_2 would be significantly improved [7].

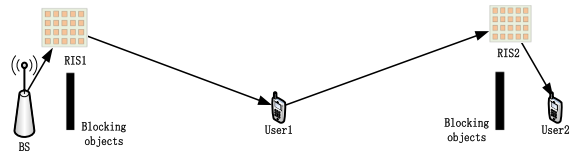

Fig. 1 A downlink RIS-aided FD CNOMA system.

2.2 Signal Model

The superposed signal transmitted by BS is $x(t) = \sqrt{a_1 P}x_1(t) + \sqrt{a_2 P}x_2(t)$, where P is the transmission power at the BS, $x_i(t)$ is the intended signal of U_i with $\mathbb{E}[|x_i|^2] = 1$, and a_i is the power allocation coefficient of U_i with the constraints $a_1 + a_2 = 1$ and $a_1 < a_2$. U_1 acting as an FD relay can not only receive the superimposed signal transmitted by the BS but also simultaneously send the decoded signal to U_2. The decoded signal for U_2 can be denoted by $s(t) = \hat{x}_2(t-\tau)$, where τ denotes the processing delay at U_1. We adopt the imperfect SI cancellation for practical implementation [8], [9], and it results in a residual loop SI. Therefore, the received signal at U_1 and U_2 can be given by $y_1(t) = d_{G_1}^{-\alpha_{G_1}/2} d_{g_1}^{-\alpha_{g_1}/2} \mathbf{G}_1 \mathbf{\Theta}_1 \mathbf{g}_1 \left(\sqrt{a_1 P}x_1(t) + \sqrt{a_2 P}x_2(t)\right) + s_I(t) + n_1(t)$ and $y_2(t) = d_{G_2}^{-\alpha_{G_2}/2} d_{g_2}^{-\alpha_{g_2}/2} \mathbf{G}_2 \mathbf{\Theta}_2 \mathbf{g}_2 \sqrt{P_r} s(t) + n_2(t)$, respectively, where d_{G_1} and d_{g_1} are the distances from the BS to R_1 and from R_1 to U_1, respectively, d_{G_2} and d_{g_2} are the distances from U_1 to R_2 and from R_2 to U_2, respectively, P_r is the transmission power of U_1, and n_i is the additive white Gaussian noise (AWGN) at U_i with zero mean and variance σ^2. Moreover, s_I is the residual SI, and it can be modeled as a Gaussian random variable with zero mean and variance $I^2 = \beta P_r^v$ [16], where $\beta > 0$ and $v \in [0,1]$. It should be noted that the values of β and v both depend on the SI cancellation scheme at U_1.

As U_2 is allocated with a higher power by the BS, the signal x_2 of U_2 can be first decoded at U_1 by treating x_1 as the interference. Thus, the received signal-to-interference-plus-noise ratio (SINR) for detecting x_2 at U_1 can be given by

$$\gamma_{1,2} = \frac{d_{G_1}^{-\alpha_{G_1}} d_{g_1}^{-\alpha_{g_1}} |\mathbf{G}_1 \mathbf{\Theta}_1 \mathbf{g}_1|^2 a_2 \rho}{d_{G_1}^{-\alpha_{G_1}} d_{g_1}^{-\alpha_{g_1}} |\mathbf{G}_1 \mathbf{\Theta}_1 \mathbf{g}_1|^2 a_1 \rho + I^2/\sigma^2 + 1}, \quad (1)$$

where $\rho = \frac{P}{\sigma^2}$ denotes the transmit SNR.

Assuming that U_1 can successfully decode the signal x_2, it can detect its own signal by adopting the SIC technique, and the corresponding SINR can be given by

$$\gamma_1 = \frac{d_{G_1}^{-\alpha_{G_1}} d_{g_1}^{-\alpha_{g_1}} \left|\mathbf{G}_1\mathbf{\Theta}_1\mathbf{g}_1\right|^2 a_1\rho}{I^2/\sigma^2+1}. \tag{2}$$

Similarly, the SNR at U_2 to detect x_2 can be given by

$$\gamma_2 = d_{G_2}^{-\alpha_{G_2}} d_{g_2}^{-\alpha_{g_2}} \left|\mathbf{G}_2\mathbf{\Theta}_2\mathbf{g}_2\right|^2 \rho_r, \tag{3}$$

where $\rho_r = \frac{P_r}{\sigma^2}$.

3. Performance Analysis

In this section, we first analyze the channel statistics for the RIS-involved reflecting links. Then, we investigate the performance of the considered system in terms of the OP and diversity order.

3.1 Channel Statistics

Based on (1)–(3), we aim for maximizing the users' SINR by intelligently adjusting the phase shifts of RISs. To this end, we derive the optimal phase shift of the n_ith element as $\theta_{i,n_i} = -arg(G_{i,n_i} g_{i,n_i})$ [11], where G_{i,n_i} and g_{i,n_i} are the n_ith element of $\mathbf{G}_i$ and $\mathbf{g}_i$, respectively. With the optimal phase shifts, we have $|\mathbf{G}_i\mathbf{\Theta}_i\mathbf{g}_i|^2 = \left(\sum_{n_i=1}^{N_i} |G_i||g_i|\right)^2$.

Lemma 1: The cumulative distribution functions (CDFs) of $X_i = |\mathbf{G}_i\mathbf{\Theta}_i\mathbf{g}_i|^2$ at low and high SNR are respectively given by

$$F_{X_i}(x) = e^{-\frac{\lambda_i}{2}} \sum_{k=0}^{\infty} \frac{\lambda^k \gamma\left(k+\frac{1}{2}, \frac{x}{2N_i(1-\epsilon_i)}\right)}{k!2^k\Gamma\left(k+\frac{1}{2}\right)}, \tag{4}$$

and

$$F_{X_i}^{0_+}(x) = \frac{\tilde{m}_i^{N_i}(4m_{s_i}m_{l_i})^{-m_{s_i}N_i}}{\Gamma(2m_{s_i}N_i)} \gamma\left(2m_{s_i}N_i, 2\sqrt{m_{s_i}m_{l_i}x}\right), \tag{5}$$

where $\epsilon_i = \frac{1}{m_{G_i}m_{g_i}}\left(\frac{\Gamma(m_{G_i}+\frac{1}{2})}{\Gamma(m_{G_i})}\right)^2\left(\frac{\Gamma(m_{g_i}+\frac{1}{2})}{\Gamma(m_{g_i})}\right)^2$, $m_{l_i} = max\{m_{G_i}, m_{g_i}\}$, $m_{s_i} = min\{m_{G_i}, m_{g_i}\}$, $\lambda_i = \frac{N_i\epsilon_i}{1-\epsilon_i}$, $\gamma(\cdot,\cdot)$ denotes the lower incomplete Gamma function and $\Gamma(\cdot)$ denotes the Gamma function.

Proof: According to [11], we can derive the CDF of $Y = \frac{\left(\sum_{n=1}^{N}|G_n||g_n|\right)^2}{N(1-\epsilon)}$ at low SNR as $F_Y(y) = e^{-\frac{\lambda}{2}}\sum_{k=0}^{\infty}\frac{\lambda^k\gamma(k+\frac{1}{2},\frac{y}{2})}{k!2^k\Gamma(k+\frac{1}{2})}$. Therefore, the CDF for $X_i = |\mathbf{G}_i\mathbf{\Theta}_i\mathbf{g}_i|^2$ at low SNR can be expressed as $F_{X_i}(x) = P_r(X_i < x) = P_r(N_i(1-\epsilon_i)Y < x) = P_r\left(Y < \frac{x}{N_i(1-\epsilon_i)}\right)$. Then, substituting $y = \frac{x}{N_i(1-\epsilon_i)}$ into the expression $F_Y(y)$, we can obtain (4).

Similarly, the CDF of $Z = \sum_{n=1}^{N}|G_n||g_n|$ at high SNR is given by $F_Z(z) = \frac{\tilde{m}^K(4m_s m_l)^{-m_s N}}{\Gamma(2m_s N)}\gamma\left(2m_s N, 2\sqrt{m_s m_l}z\right)$. Hence, the CDF for X_i at high SNR can be expressed as $F_{X_i}(x) = P_r(X_i < x) = P_r(Z^2 < x) = P_r\left(Z < \sqrt{x}\right)$. Then, substituting $z = \sqrt{x}$ into the expression $F_Z(z)$, we can obtain (5). This proofs Lemma 1.

3.2 Outage Probability

Next, we continue to investigate the OP performance of the two users. For U_1, the outage occurs when U_1 cannot decode x_2 or fails to detect its own message x_1. Then, we can derive the OP of U_1 through its complementary events, which can be given by

$$P_1 = 1 - P_r(\gamma_{1,2} \geq \tilde{\gamma}_2, \gamma_1 \geq \tilde{\gamma}_1), \tag{6}$$

where $\tilde{\gamma}_i = 2^{\tilde{R}_i} - 1$, and $\tilde{R}_i$ is the predefined target data rate of U_i. For U_2, the outage occurs when U_1 cannot decode x_2 or U_2 cannot detect its own message x_2. Similarly, the OP of U_2 can be given by

$$P_2 = 1 - P_r(\gamma_{1,2} \geq \tilde{\gamma}_2, \gamma_2 \geq \tilde{\gamma}_2). \tag{7}$$

According to Lemma 1, We proceed to derive the OP expressions for U_1 and U_2 in the following theorem.

Theorem 1: The closed-form expressions for the OPs of U_1 and U_2 are given by

$$P_1 = \begin{cases} F_{X_1}\left(\tilde{\rho}_{1,2}\right), & \frac{\tilde{\gamma}_1}{\tilde{\gamma}_1+\tilde{\gamma}_2+\tilde{\gamma}_1\tilde{\gamma}_2} < a_1 < \frac{1}{1+\tilde{\gamma}_2}, \\ F_{X_1}\left(\tilde{\rho}_1\right), & 0 < a_1 < \frac{\tilde{\gamma}_1}{\tilde{\gamma}_1+\tilde{\gamma}_2+\tilde{\gamma}_1\tilde{\gamma}_2}, \\ 1, & otherwise, \end{cases} \tag{8}$$

and

$$P_2 = F_{X_1}\left(\tilde{\rho}_{1,2}\right) + F_{X_2}\left(\tilde{\rho}_2\right) - F_{X_1}\left(\tilde{\rho}_{1,2}\right)F_{X_2}\left(\tilde{\rho}_2\right), \tag{9}$$

respectively, where $\tilde{\rho}_{1,2} = \frac{I_0\tilde{\gamma}_2}{b(a_2-a_1\tilde{\gamma}_2)\rho}$, $\tilde{\rho}_1 = \frac{I_0\tilde{\gamma}_1}{ba_1\rho}$, and $\tilde{\rho}_2 = \frac{\tilde{\gamma}_2}{c\rho_r}$ with $I_0 = I^2/\sigma^2+1, b = d_{G_1}^{-\alpha_{G_1}}d_{g_1}^{-\alpha_{g_1}}$, and $c = d_{G_2}^{-\alpha_{G_2}}d_{g_2}^{-\alpha_{g_2}}$.

Proof: For U_1, we have $P_1 = 1 - P_r(\gamma_{1,2} \geq \tilde{\gamma}_2, \gamma_1 \geq \tilde{\gamma}_1) = 1 - P_r\left(X_1 > max\left(\frac{I_0\tilde{\gamma}_2}{bP(a_2-a_1\tilde{\gamma}_2)}, \frac{I_0\tilde{\gamma}_1}{ba_1P}\right)\right)$. When $\frac{\tilde{\gamma}_1}{\tilde{\gamma}_1+\tilde{\gamma}_2+\tilde{\gamma}_1\tilde{\gamma}_2} < a_1 < \frac{1}{1+\tilde{\gamma}_2}$, $\tilde{\rho}_{1,2} > \tilde{\rho}_1$. In this case, we can easily derive the OP of U_1 as $F_{X_1}\left(\tilde{\rho}_{1,2}\right)$. Similarly, for the case of $0 < a_1 < \frac{\tilde{\gamma}_1}{\tilde{\gamma}_1+\tilde{\gamma}_2+\tilde{\gamma}_1\tilde{\gamma}_2}$, i.e., $\tilde{\rho}_{1,2} > \tilde{\rho}_1$, we can obtain the OP of U_1 as $F_{X_1}\left(\tilde{\rho}_1\right)$. For U_2, according to (7), we have $P_2 = P_r(\gamma_{1,2} < \tilde{\gamma}_2) + P_r(\gamma_2 < \tilde{\gamma}_2) - P_r(\gamma_{1,2} < \tilde{\gamma}_2)P_r(\gamma_2 < \tilde{\gamma}_2)$. After some algebraic manipulations, we can obtain the OP of U_2 as (9). This proofs Theorem 1.

Remark 1: According to simulation results shown in Section 4, the expressions (8) and (9) for the OPs of U_1 and U_2 are accurate at low SNR, while the OPs at high SNR need to be derived from expression (5).

Remark 2: According to Theorem 1, we can observe that both $\tilde{\rho}_1$ and $\tilde{\rho}_{1,2}$ vary with the SI, which also shows that the OP of U_i is significantly effected by the SI.

3.3 Asymptotic OP and Diversity Analysis

To gain more insights, we proceed to analyze the asymptotic

OPs and diversity orders at high SNR.

Theorem 2: In the high-SNR regime, P_1 and P_2 can be approximated as

$$P_1^{\infty} = \begin{cases} \frac{\tilde{m}_1{}^{N_1}\tilde{\rho}_{1,2}^{m_{s_1}N_1}}{\Gamma(2m_{s_1}N_1+1)}, & \frac{\tilde{\gamma}_1}{\tilde{\gamma}_1+\tilde{\gamma}_2+\tilde{\gamma}_1\tilde{\gamma}_2} < a_1 < \frac{1}{1+\tilde{\gamma}_2}, \\ \frac{\tilde{m}_1{}^{N_1}\tilde{\rho}_1^{m_{s_1}N_1}}{\Gamma(2m_{s_1}N_1+1)}, & 0 < a_1 < \frac{\tilde{\gamma}_1}{\tilde{\gamma}_1+\tilde{\gamma}_2+\tilde{\gamma}_1\tilde{\gamma}_2}, \\ 1, & otherwise, \end{cases} \tag{10}$$

and

$$P_2^{\infty} = \frac{\tilde{m}_1{}^{N_1}\tilde{\rho}_{1,2}^{m_{s_1}N_1}}{\Gamma(2m_{s_1}N_1+1)} + \frac{\tilde{m}_2{}^{N_2}\tilde{\rho}_2^{m_{s_2}N_2}}{\Gamma(2m_{s_2}N_2+1)}, \tag{11}$$

respectively.

Proof: Since users' OPs at high SNR can be obtained through (5), a corresponding approximation study is conducted on it. First, we expand the lower incomplete gamma and exponential functions in (5), and then derive $F_{X_i}^{0_+}(x) = \tilde{m}_i{}^{N_i}\sum_{l=0}^{\infty}\frac{(2\sqrt{m_{s_i}m_{l_i}})^l x^{m_{s_i}N_i+\frac{l}{2}}}{\Gamma(l+2m_{l_i}N_i+1)}\sum_{k=0}^{\infty}\frac{(-2\sqrt{m_{s_i}m_{l_i}}x)^k}{k!}$. Next, we extract the lowest-order terms, and the approximation can be expressed as $F_{X_i}^{0_+}(x) \approx \frac{\tilde{m}_i{}^{N_i}x^{m_{s_i}N_i}}{\Gamma(2m_{l_i}N_i+1)}$. Based on this, the asymptotic OP of U_1 can be obtained as (10). For U_2, according to (7) and conducting some algebraic manipulations, we have $P_2 = F_{X_1}^{0_+}(\tilde{\rho}_{1,2}) + F_{X_2}^{0_+}(\tilde{\rho}_2) - F_{X_1}^{0_+}(\tilde{\rho}_{1,2})F_{X_2}^{0_+}(\tilde{\rho}_2)$. By extracting the lowest-order terms, we derive the expression (11). This completes the proof of Theorem 2.

Remark 3: According to Theorem 2, we can observe that the diversity order of U_i is determined by the number of RIS elements, the SI of FD relaying, and Nakagami fading parameters of channels.

Corollary 1: If the perfect SI cancellation is applied at U_1, we can obtain that the diversity order of U_1 is $m_{s_1}N_1$, and the diversity order of U_2 is $min(m_{s_1}N_1, m_{s_2}N_2)$.

Proof: According to (10), we can obviously observe that the diversity gain of U_1 is $m_{s_1}N_1$. For U_2, when $m_{s_1}N_1 \le m_{s_2}N_2$, the lower-order term in expression (11) is $\frac{\tilde{m}_1{}^{N_1}\tilde{\rho}_{1,2}^{m_{s_1}N_1}}{\Gamma(2m_{s_1}N_1+1)}$, based on which the diversity order of U_2 is $m_{s_1}N_1$. Similarly, when $m_{s_1}N_1 \ge m_{s_2}N_2$, the lower-order term in expression (11) is $\frac{\tilde{m}_2{}^{N_2}\tilde{\rho}_2^{m_{s_2}N_2}}{\Gamma(2m_{s_2}N_2+1)}$, and the diversity order of U_2 is $m_{s_2}N_2$. Thus, we can derive the diversity order of U_2 is $min(m_{s_1}N_1, m_{s_2}N_2)$. This proofs Corollary 1.

4. Numerical Results

In this section, numerical results are presented to evaluate the performance of our proposed system. The parameter settings are shown in Table 1. Here, we adopt 1 MHz bandwidth, which can be applied in video transmission with general resolution or real-time voice communication [11], [17]. In addition, we assume $P_r = P$.

Figure 2 plots the users' OPs versus the transmit SNR with the number of RIS elements $N = 10, 20$, and 30, where

Table 1 Parameters setting.

Bandwidth	BW=1 MHz
Distances	d_{G_1}=10m, d_{g_1}=80 m, d_{G_2}=60 m, and d_{g_2}=1 0m
Path-loss exponent	$\alpha_{g_i}=\alpha_{G_i}$=2.5
Nakagami fading parameters	m_{g_i}=1 and m_{G_i}=3
Target data-rates	$\tilde{R}_1=\tilde{R}_2$=0.1 Mbps
Power-allocation coefficients	a_1=0.4 and a_2=0.6
Self-interference parameters	$\beta = 10^{-3}$ and $v = 0.1$

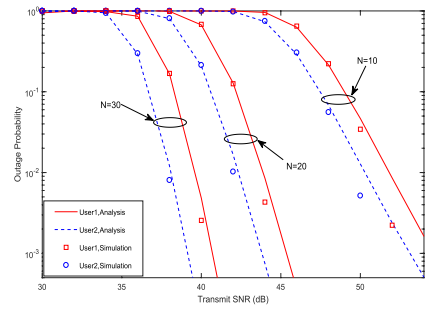

Fig. 2 OPs versus the transmit SNR with $N_1 = N_2 = N$.

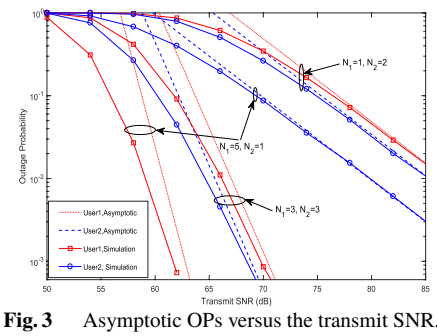

Fig. 3 Asymptotic OPs versus the transmit SNR.

we assume $N_1 = N_2 = N$. From this figure, we can observe that the analyses derived from (8) and (9) are accurate at low SNR, which is consistent with the conclusion of Remark 1. In addition, we can see that the OPs of two users decrease as N increases. It is because the channel gain increases with the number of RIS elements.

Figure 3 further plots the high-SNR approximation curves with different N_1 and N_2 conditions, where we assume the perfect SI cancellation is adopted. From this figure, we can observe that users' OPs gradually approach their corresponding approximate curves, which perfectly matches the analytical results derived in (10) and (11). By observing the curves, we can obtain that for the three cases: 1) $N_1 = 1, N_2 = 2$, 2) $N_1 = N_2 = 3$, and 3) $N_1 = 5, N_2 = 1$, the diversity orders of U_1 are 1, 3, and 5, respectively, while the diversity orders of U_2 are equal to 1, 3, and 1, respectively. The above results verify the conclusion of Corollary 1.

Figure 4 presents the effect of FD SI on the outage performance and compares the RIS-aided FD CNOMA scheme with the HD CNOMA scheme. From this figure, we can see that FD SI has a significant impact on the users' outage performance. Specifically, the OP is significantly reduced by decreasing the residual SI. In contrast, with the increase of residual SI, the advantage of FD CNOMA no longer exists. Therefore, it is important to employ effective SI cancellation techniques for the RIS-aided FD CNOMA scheme.

Figure 5 plots the OPs versus the transmit SNR under

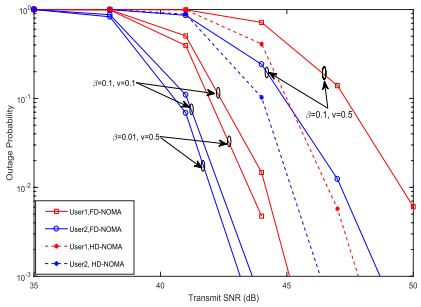

Fig. 4 The impact of SI on the OP.

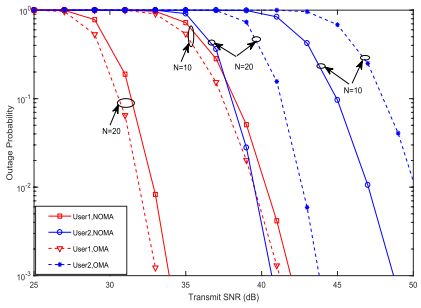

Fig. 5 OPs versus the transmit SNR under both NOMA and OMA schemes.

both the NOMA and OMA schemes with $v = 0.001$. Specially, the locations of the two users are set to $d_{g_1} = 30\,m$ and $d_{G_2} = 80\,m$. From this figure, we can observe that the performance of U_1 in the NOMA scheme is close to that in OMA scheme, while the performance of U_2 in the NOMA scheme is much better than that in OMA scheme. Comprehensively, the NOMA scheme outperforms the OMA scheme under specific parameter settings. Moreover, in this considered scenario, the performance of U_1 is better than that of U_2, which is different from Fig. 2. It is because the performance of the two users is relatively independent and varies with their associated parameters.

5. Conclusion

In this paper, we proposed a novel RIS-aided FD CNOMA scheme to enhance the coverage extension for the far user, where the near user acts as an FD, and two RISs are employed to establish corresponding reflecting links for the paired users respectively. Furthermore, we investigated the transmit reliability of our proposed network in terms of the OP and diversity order. Specifically, we first analyzed the corresponding channel statistics of reflecting links. Then, we derived the closed-form expressions of the OP for both users. To gain further insights, we analyzed the asymptotic OP and obtained the diversity orders at high SNR. Numerical results were presented to validate our analysis, which reveals that users' diversity orders are affected by their channel fading parameters, the SI of FD, and the number of RIS elements.

Acknowledgments

This work was supported in part by the National Natural Science Foundation of China under Grants 62071242 and 62071005, in part by the Natural Science Foundation of Anhui Province under Grant 2008085MF181, and in part by the Innovation Program of Graduate Education of Jiangsu Province of China under Grant KYCX200737.

References

[1] Q. Wu, S. Zhang, B. Zheng, C. You, and R. Zhang, "Intelligent reflecting surface aided wireless communications: A tutorial," IEEE Trans. Commun., vol.69, no.5, pp.3313–3351, May 2021.

[2] B. Lyu, P. Ramezani, D.T. Hoang, S. Gong, Z. Yang, and A. Jamalipour, "Optimized energy and information relaying in self-sustainable IRS-empowered WPCN," IEEE Trans. Commun., vol.69, no.1, pp.619–633, Jan. 2021.

[3] Q. Wu and R. Zhang, "Intelligent reflecting surface enhanced wireless network via joint active and passive beamforming," IEEE Trans. Wireless Commun., vol.18, no.11, pp.5394–5409, Nov. 2019.

[4] H. Guo, Y.-C. Liang, J. Chen, and E.G. Larsson, "Weighted sum-rate maximization for reconfigurable intelligent surface aided wireless networks," IEEE Trans. Wireless Commun., vol.19, no.5, pp.3064–3076, May 2020.

[5] L. Dai, B. Wang, Y. Yuan, S. Han, I. Chih-lin, and Z. Wang, "Non-orthogonal multiple access for 5G: Solutions, challenges, opportunities, and future research trends," IEEE Commun. Mag., vol.53, no.9, pp.74–81, Sept. 2015.

[6] Y. Feng, S. Yan, Z. Yang, N. Yang, and J. Yuan, "Safeguarding non-orthogonal multiple access with physical-layer techniques," IEEE Netw., vol.36, no.3, pp.145–151, May/June 2022.

[7] Z. Zhang, Z. Ma, M. Xiao, Z. Ding, and P. Fan, "Full-duplex device-to-device-aided cooperative nonorthogonal multiple access," IEEE Trans. Veh. Technol., vol.66, no.5, pp.4467–4471, May 2017.

[8] X. Yue, Y. Liu, S. Kang, A. Nallanathan, and Z. Ding, "Exploiting full/half-duplex user relaying in NOMA systems," IEEE Trans. Commun., vol.66, no.2, pp.560–575, Feb. 2018.

[9] L. Zhang, J. Liu, M. Xiao, G. Wu, Y. Liang, and S. Li, "Performance analysis and optimization in downlink NOMA systems with cooperative full-duplex relaying," IEEE J. Sel. Areas Commun., vol.35, no.10, pp.2398–2412, Oct. 2017.

[10] Z. Ding and H. Vincent Poor, "A simple design of IRS-NOMA transmission," IEEE Commun. Lett., vol.24, no.5, pp.1119–1123, May 2020.

[11] Y. Cheng, K.H. Li, Y. Liu, K.C. Teh, and H. Vincent Poor, "Downlink and uplink intelligent reflecting surface aided networks: NOMA and OMA," IEEE Trans. Wireless Commun., vol.20, no.6, pp.3988–4000, June 2021.

[12] J. Zuo, Y. Liu, and N. Al-Dhahir, "Reconfigurable intelligent surface assisted cooperative non-orthogonal multiple access systems," IEEE Trans. Commun., vol.69, no.10, pp.6750–6764, Oct. 2021.

[13] M. Elhattab, M.A. Arfaoui, C. Assi, and A. Ghrayeb, "Reconfigurable intelligent surface enabled full-duplex/half-duplex cooperative non-orthogonal multiple access," IEEE Trans. Wireless Commun., vol.21, no.5, pp.3349–3364, May 2022.

[14] D. Li, "How many reflecting elements are needed for energy- and spectral-efficient intelligent reflecting surface-assisted communication," IEEE Trans. Commun., vol.70, no.2, pp.1320–1331, Feb. 2022.

[15] Z. Xing, R. Wang, J. Wu, and E. Liu, "Achievable rate analysis and phase shift optimization on intelligent reflecting surface with hardware impairments," IEEE Trans. Wireless Commun., vol.20, no.9, pp.5514–5530, Sept. 2021.

[16] L.J. Rodriguez, N.H. Tran, and T. Le-Ngoc, "Performance of full-duplex AF relaying in the presence of residual self-interference," IEEE J. Sel. Areas Commun., vol.32, no.9, pp.1752–1764, Sept. 2014.

[17] Z. Tang, T. Hou, Y. Liu, J. Zhang, and L. Hanzo, "Physical layer security of intelligent reflective surface aided NOMA networks," IEEE Trans. Veh. Technol., vol.71, no.7, pp.7821–7834, July 2022.